PNAS RESEARCH ARTICLE | ENGINEERING

Plant cell-like tip-growing polymer precipitate with structurally embedded multistimuli sensing ability

Chan Jin Park[a], Jonghyun Ha[a,b], Hae-Ryung Lee[c], Keunhwan Park[d,1], Jeong-Yun Sun[c,e,1], and Ho-Young Kim[a,1]

Edited by Rayne Xiaoyu Zheng, University of California–Los Angeles; received July 3, 2022; accepted November 23, 2022 by Editorial Board Member Yonggang Huang

Soft systems that respond to external stimuli, such as heat, magnetic field, and light, find applications in a range of fields including soft robotics, energy harvesting, and biomedicine. However, most of the existing systems exhibit nondirectional, nastic movement as they can neither grow nor sense the direction of stimuli. In this regard, artificial systems are outperformed by organisms capable of directional growth in response to the sense of stimuli or tropic growth. Inspired by tropic growth schemes of plant cells and fungal hyphae, here we report an artificial multistimuli-responsive tropic tip-growing system based on nonsolvent-induced phase separation of polymer solution, where polymer precipitates as its solvent dissolves into surrounding nonsolvent. We provide a theoretical framework to predict the size and velocity of growing precipitates and demonstrate its capability of sensing the directions of gravity, mechanical contact, and light and adjusting its growing direction in response. Exploiting the embedded physical intelligence of sensing and responding to external stimuli, our soft material system achieves multiple tasks including printing 3D structures in a confined space, bypassing mechanical obstacles, and shielded transport of liquids within water.

tip growth | polymer precipitation | biomimetics | physical intelligence

Significance

Here, we report a technology to grow a polymer structure, which can adapt its growing direction in response to environmental stimuli. Inspired by tip-growing cells like pollen tube and fungal hyphae, our artificial system grows from tips as polymer precipitates but requires much weaker pressure than the natural counterparts. We demonstrate various applications, including printing 3D structures in a confined space, autonomously bypassing mechanical obstacles, and transporting liquids underwater in a shielded manner. In addition to suggesting a material system for novel soft robots that can autonomously interact with the surrounding environments, our bioinspired growing system serves as a tool to enhance physical understanding of nature's tip-growing cells.

Implementing the adaptability of living organisms in an artificial system is a topic of significant interest in soft robotics, (1–4) energy harvesting, (5) and biomedicine (2, 4, 6). A range of materials that expand, shrink, stiffen, or soften in response to environmental stimuli like heat, magnetic field, electric field, light, and humidity have been developed to perform programmed tasks (1–5). However, mostly responding in a nondirectional manner as they lack the ability to sense the direction of the stimulus, artificial stimulus-responsive systems are still frequently outperformed by living organisms, which conduct diverse challenging tasks while sensing the directions of various stimuli imposed from the environments. For example, while navigating their environments through growth as shown in Fig. 1*A*, some plants can sense the direction of gravity and grow along or against the direction, a behavior termed gravitropism (Fig. 1*B*) (7). Many plants sense and respond to the direction of light or exhibit phototropism, by either growing toward or away from the light (Fig. 1*C*) (8). Similarly, some plants can sense and respond to the mechanical contact (Fig. 1*D*), exhibiting thigmotropism (9, 10). Tropic growth, the directional growth in response to the directional stimuli, allows the plants and fungi to adapt to the surrounding environments. Developing artificial systems equipped with this trait will allow us to build innovative robots that can actively adapt their shapes and movements to the environments for medical, industrial, military, and environmental applications. In addition, building and scrutinizing artificial tropic growth systems can enhance our understandings of nature's tropic growth, in turn.

We first consider the fundamental physical mechanism underpinning the tropic tip growth of plants and fungi. Plant cells or fungal hyphae grow through expansion, which is driven by the internal turgor pressure while resisted by cell wall strength (11). Although turgor pressure has no preferential direction as a scalar quantity, some cells can grow in an anisotropic manner. For example, as shown in Fig. 1*A*, pollen tubes can guide the growth to occur only at its tip by locally reducing the cell wall strength at the tip (12, 13). Such tip growth is adopted in various cells from different kingdoms including protonemata and root hairs of plants and hyphae of fungi. Adopting the identical growth scheme, those tip-growing cells exhibit a similar shape of a long cylindrical body topped with a semi-spheroidal tip. Tip growth offers multiple advantages including rapid and precise direction adjustment in response to external signals and energy efficiency (14). It is widely perceived that the following three conditions are necessary for tip growth to occur: i) cell wall strength gradient in the meridional direction with the lowest strength at the apex, ii) sufficiently large turgor pressure to expand the cell wall, and iii) tip-targeted cytoplasmic streaming

Author contributions: K.P., J.-Y.S. and H.-Y.K. designed research; C.J.P., J.H., and H.-R.L. performed research; C.J.P., J.H., H.-R.L., K.P., J.-Y.S., and H.-Y.K. analyzed data; and C.J.P., J.H., K.P., J.-Y.S., and H.-Y.K. wrote the paper.

Competing interest statement: The authors declare a competing interest. The authors have patent filings to disclose. H.-Y.K. and C.J.P. are the inventors on the patent applications (#10-2020-0142306, Republic of Korea) submitted by SNU R&DB Foundation that covers manufacturing method of growing body and its applications.

This article is a PNAS Direct Submission. R.X.Z. is a guest editor invited by the Editorial Board.

[1]To whom correspondence may be addressed. Email: kpark@gachon.ac.kr, jysun@snu.ac.kr, or hyk@snu.ac.kr.

This article contains supporting information online at https://www.pnas.org/lookup/suppl/doi:10.1073/pnas.2211416120/-/DCSupplemental.

Published January 3, 2023.

which provides expanding cell wall with building blocks and prevents thinning of the cell wall (13).

Inspired by this tip-growing strategy of nature, here, we developed a system that can mimic tip growth by simultaneously satisfying the aforementioned three conditions using nonsolvent-induced phase separation (NIPS) of a cellulose acetate (CA)–acetone solution. Because the CA precipitate grows in an analogous manner to the tip-growing cells, it possesses pollen tube-like morphology—a long cylinder topped with prolate semispheroidal tip as shown in Fig. 1*E* (Movie S1). Moreover, similar to the plant cells, the growing CA precipitate adjusts its direction in response to the applied external stimuli, i.e., gravity, light, and mechanical contact, thereby exhibiting gravitropism, phototropism, and thigmotropism. Tropic characteristics allow us to steer the growing precipitate using various stimuli as depicted in the first three panels of Fig. 1*F*. In addition to the growing direction, the size of the precipitate can also be precisely controlled by varying the internal pressure as illustrated in the fourth panel of Fig. 1*F*. Finally, as shown in the rightmost panel of Fig. 1*F*, the growing precipitate can be used as a conduit for shielded underwater transport of liquids.

Results

Conditions for Tip Growth. Tip-growing of CA precipitate is achieved by extruding the CA–acetone solution inside a bath of water as shown in Fig. 1*E*, the experiment carried out in a setup illustrated in Fig. 2*A*. The extruded polymer solution rises to form an opaque cylinder with a transparent, prolate semispheroidal tip via NIPS. As shown in Fig. 2*A*, when the transparent solution contacts water, the solution rapidly transforms to a transparent gel at the interface as significant amount of solvent, acetone, immediately diffuses out into the water (15). Through continuous deprival of acetone and invasion of water, the inner solution near the gel layer eventually turns into an opaque solid of CA when the CA concentration crosses binodal curve giving rise to phase separation (*SI Appendix*, Supplementary Discussion S1) (16). Therefore, always transparent tip indicates that fresh solution is continuously replenished at the growing tip to lower the CA concentration.

Because acetone and water are gradually exchanged at the solution–water interface, gel's viscosity at the tip, which provides the wall strength, increases monotonically along the meridional direction (17, 18) and establishes wall strength gradient. The high internal pressure coming from extrusion expands the semispheroidal tip but the expansion is ceased at the equator as the viscosity increases. This is verified by visualizing the internal flow through particle tracking velocimetry, in which fluorescent particles seeded in the solution are tracked during growth (Movie S1). As shown in the top right picture of Fig. 2*A*, similar to the tip-growing cells that exhibit orthogonal growth at the tip (19), the fresh solution within the tip flows orthogonal to the tip interface, consistent with the trajectory predicted by a mathematical model (*SI Appendix*, Supplementary Discussion S2).

The outer phase-separated layer at the stalk guides the internal flow toward the continually advancing tip. This is also confirmed by internal flow visualization in Fig. 2*A*, which clearly shows that the fresh solution flows toward the tip with negligible radial velocity in the cylindrical stalk. The scanning electron microscopy (SEM) image in the bottom right of Fig. 2*A* shows the cross section of the resulting hollow cylinder of CA. Therefore, the aforementioned three conditions required for tip growth (13) can be met by extruding various polymer solutions undergoing NIPS in a nonsolvent (*SI Appendix*, Supplementary Discussion S3).

The tip growth is only achieved within limited ranges of CA concentration and extruded flow rate as shown in the regime map of Fig. 2*B*, where the red dots denote the tip-growing condition. Otherwise, the extruded solution grows from the nozzle (base) with its tip solidifying first (*Left Inset*), in contrast to the tip-growing solution (*Right Inset*). This is because the tip growth of polymer solution is only possible when the wall strength at the tip, a function

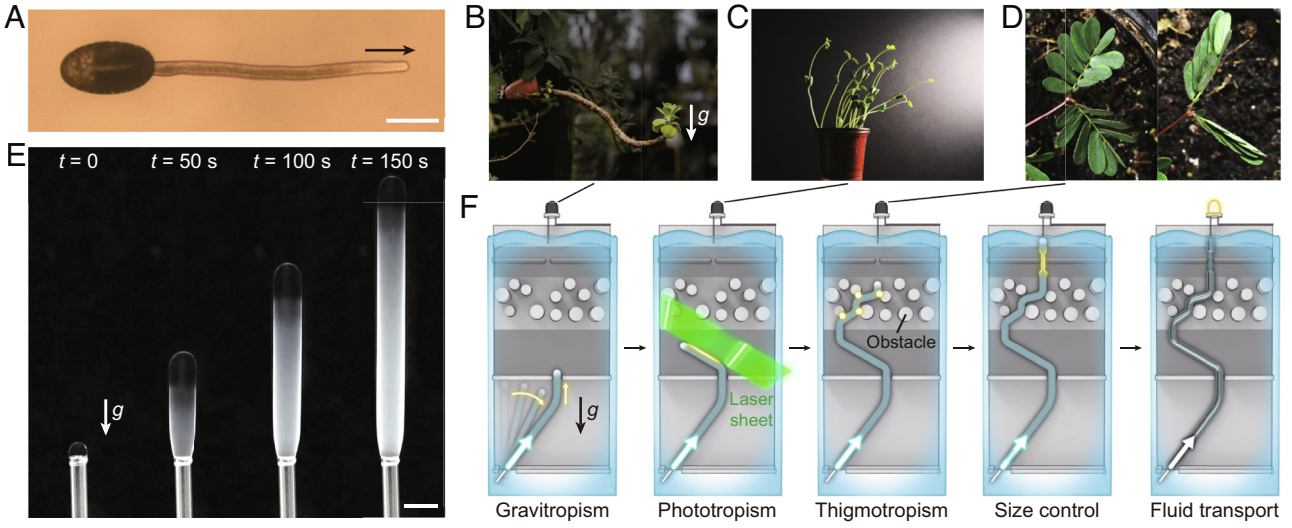

Fig. 1. Tip-growing polymer precipitate and its tropic characteristics. (*A*) A pollen tube of lily, *Lilium longiflorum*, germinated from a pollen grain. A long cylindrical cell grows out of the pollen with the growth limitedly occurring at the tip. Growing direction of the pollen tube is denoted by a black arrow. (Scale bar, 50 μm.) (*B*) Gravitropism of *Aeonium arboreum* leaves. The leaves grow in the direction against the gravity. (*C*) Phototropism of *Glycine max* sprouts. The sprouts grow toward the light. (*D*) *Mimosa pudica* leaves before applying touch stimulus (*Left*) and after applying the stimulus (*Right*). The leaves fold when touched. (*E*) Tip-growing of CA precipitate in water. As the solution is continuously fed, the opaque cylinder elongates while the growing tip remains transparent. $t = 0$ corresponds to the initiation of solution extrusion. (Scale bar, 3 mm.) (*F*) Tropic characteristics and functions of our system. Similar to the plant cells, the growing precipitate can sense gravity, light, and physical contact and change growing direction in response. This allows the precipitate to bypass obstacles and grow toward a target (lead of a LED). The size of the precipitate can be precisely controlled, and therefore, it can pass a small gap. The grown precipitate can be used as a fluid conduit to transport fluid in a shielded manner, and by transporting conductive fluid, the precipitate can be used as a growing wire that completes an electronic circuit underwater.

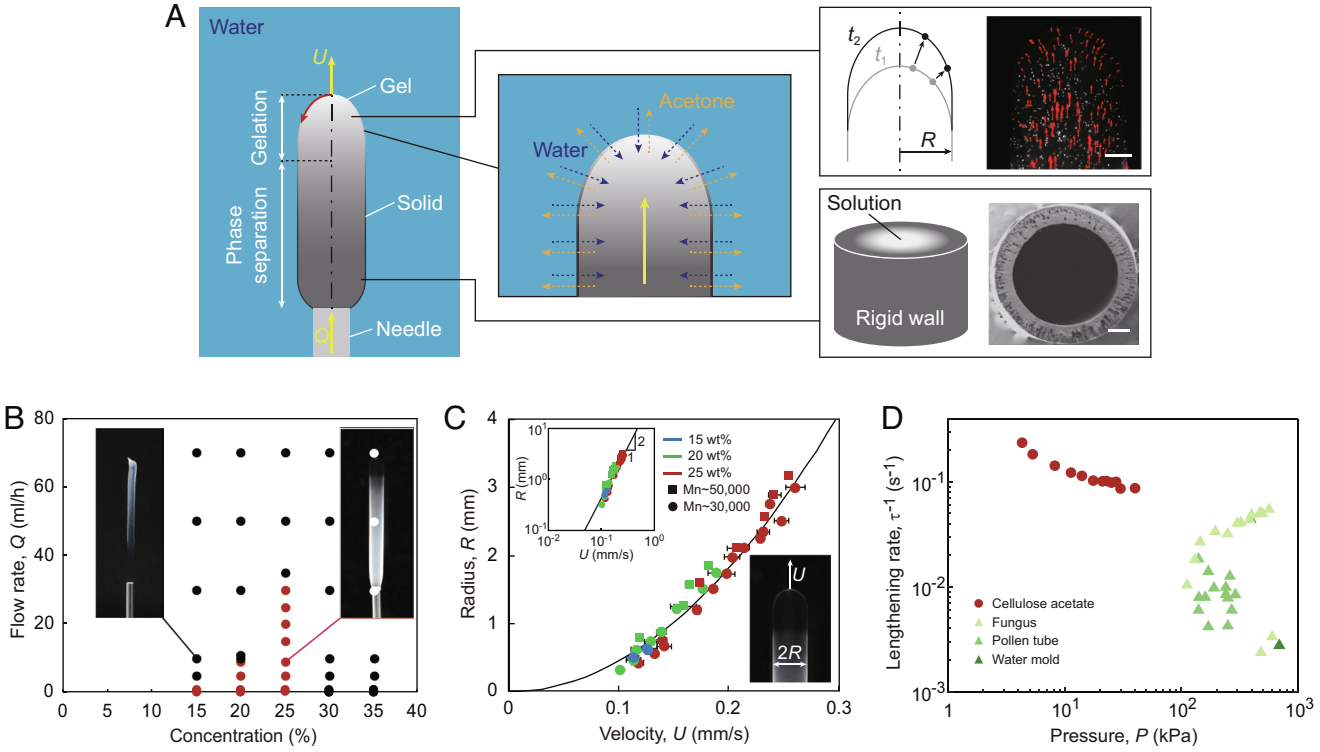

Fig. 2. Tip-growing condition and growth dynamics. (*A*) Schematic illustration of the experimental setup (*Left*), solvent–nonsolvent exchange in the tip during growth (*Middle*), internal flow visualization using fluorescent particles (*Top Right*), and SEM image of the growing precipitate (*Bottom Right*). Red arrow in the left schematic denotes the meridional direction. The cylinder in the SEM image was obtained by first replacing the internal fresh solution with liquid metal during growth and then rinsing the liquid metal away after the cylinder is solidified. (Scale bars, 300 μm.) (*B*) Regime map of tip-growing (*Right Inset* image) and basal-growing (*Left Inset* image) conditions of extruded CA solution. Red and black dots denote tip-growing conditions and basal-growing conditions, respectively. (Scale bars, 3 mm.) (*C*) Experimentally measured radius of the tip-growing precipitate, *R* versus growth rate, *U*. Black line stands for $y = 45x^2$. *Inset*: log–log plot of *R* versus *U*. Line with a slope of 2 is shown together with the data points in the *Inset*. (*D*) Lengthening rate τ^{-1} of various tip-growing cells in nature versus the pressure that drives the growth. Data and references are provided in *SI Appendix*, Table S1. Each data point is the average of three measurements, and error bars correspond to the SD (*C* and *D*). Error bar is smaller than the size of the symbols in *D*.

of CA concentration, balances the internal pressure, determined by the flow rate. If the wall is too strong, or the solution turns into solid too rapidly due to high solution concentration (20), the internal pressure cannot deform the wall and therefore basal growth rather than tip growth arises. If the wall is too weak to withstand the internal pressure owing to the high flow rate, the tip bursts as in over-pressurized tip-growing plant cells (*SI Appendix*, Supplementary Discussion S4) (21). The burst pressure, or maximum flow rate for tip growth, increases with increasing solute concentration because solution's viscosity increases with solute concentration. Growth is not observed when extruding solutions with low concentrations, below 15 wt%, where no solid structures can be formed (22). Previous studies on extrusion of CA–acetone solution in water using similar experimental setups failed to achieve tip growth because they usually extruded the solution very fast, thereby causing solidification to initially occur at the tip (23, 24).

Growth Dynamics. The growing precipitate's diameter is controlled by the extruded flow rate while being independent of the extruding nozzle size (*SI Appendix*, Supplementary Discussion S5), which allows us to grow structures whose size vary significantly in a single setup. This is in contrast with typical fluid jets whose size is determined by the nozzle—only the jet velocity varies when the flow rate is altered. This is because as mentioned above, tip growth from the solution is achieved by the balance between the wall strength at the tip and internal pressure. With increasing flow rate, the internal pressure increases, which in turn promotes expansion of outer gel layer at the tip, resulting in increased radius. For solutions that contain CA with different average molecular weights as a solute, we varied extrusion flow rates to obtain the relationship between the radius of growing precipitate, *R*, and the growth rate of cylinder length, *U*, $R \sim U^2$ as shown in Fig. 2*C*. We found that change in the molecular weight of the solute exerts an insignificant effect on the size of the growing CA precipitate. When two CA precipitates growing from different nozzles come close to each other at their tips, they merge and then regrow from a single tip (*SI Appendix*, Supplementary Discussion S6) similar to the fusion observed in fungal hyphae (25, 26). The size of the merged tip is also determined by the sum of the two flow rates.

We now rationalize the above empirical relation between *R* and *U*. As the pressure governs growth, we first measured the pumping gauge pressure, *P*, in the syringe pump for different flow rates, to find $R \sim \sqrt{P}$ (*SI Appendix*, Supplementary Discussion S7). As the tip growth of CA shares the similar physical mechanism to that of tip-growing cells in nature, we apply the corresponding biomechanical theory to the tip growth of CA solution (27, 28). Because the tip expands orthogonal to its own interface (*SI Appendix*, Supplementary Discussion S2), the geometry of the tip represented by the ratio between two principal curvatures can be expressed using a single flow coupling variable, $\nu(s)$, such that $\kappa_s(s)/\kappa_\theta(s) = 1 - 2\nu(s)$, where *s* is the meridional position, $\kappa_s(s)$ is principal curvature in meridional direction, and $\kappa_\theta(s)$ is curvature in circumferential direction (27). While the radius of the precipitate increases with the flow rate, the tip is always a prolate semispheroid with the major axis being 1.3 times longer than the minor axis (*SI Appendix*, Supplementary Discussion S8). This is because flow coupling variable $\nu(s)$, analogous to Poisson's ratio in elasticity, is determined by the polymer solution (27).

As every tip of the growing precipitate assumes a similar shape, they must have identical nondimensional strain rate on the identical position when we nondimensionalize the tip geometry using the radius R. To calculate the strain rate, we consider the constitutive equation of $\dot{\epsilon} = \sigma / \mu$, where $\dot{\epsilon}$ is the strain rate, σ is the stress, and μ is the gel viscosity. Although typical plant cell walls behave like Bingham plastic, (29) we use the constitutive equation for viscous cell walls (28) because the yield stress of our growing solution is less than 4 kPa, an insignificant value compared to the extrusion pressure (*SI Appendix*, Supplementary Discussion S7). From axial force balance, meridional strain rate at the tip $\dot{\epsilon}_s$ is written as (27, 28),

$$\dot{\epsilon}_s = \frac{P}{2\mu\kappa_\theta\delta},$$

where δ is the wall thickness that increases proportional to the square root of water contact time because acetone–water exchange is diffusion-driven (*SI Appendix*, Supplementary Discussion S9) (30).

Here, μ depends on water contact time t because μ increases as acetone–water exchange proceeds. We consider time-varying viscosity $\mu \sim t^\alpha$, as in thermosetting polymers, where α is a fitting parameter (31, 32). As every tip has a similar shape, the distance the solution travels from the apex of the tip before being deposited at the equator, is proportional to the tip radius R. Therefore, given the self-similar nature of the tip growth, the time required for the fresh solution at the apex of the tip to reach the equator is proportional to the characteristic time $\tau = R/U$, and the nondimensional strain rate is given by $\dot{\epsilon}_s\tau$. Substituting $P \sim R^2$, $\mu \sim \tau^\alpha$, $\kappa_\theta \sim 1/R$, and $\delta \sim \tau^{0.5}$ into $\dot{\epsilon}_s\tau$, we obtain the relation between the cylinder radius R and the growth rate U that the growing precipitate must satisfy to fulfill the identical nondimensional strain rate condition, $R^{(\alpha-3.5)} \sim U^{(\alpha-0.5)}$. For $\alpha = 6.5$, we get $R \sim U^2$, which matches our experimental observation, noting that α ranges typically from 4 to 8 (32). We also provide a theoretical model to predict the length of the transparent region at the tip of the growing precipitate (*SI Appendix*, Supplementary Discussion S10).

To compare our tip-growing precipitate with tip-growing cells, we consider the lengthening rate defined by $\tau^{-1} = U/R$, and pressure P driving the growth in a given system (33). As shown in Fig. 2*D*, cells adopt large turgor pressure, at least a few hundred kPa, to grow (34, 35). In contrast, tip growth of precipitate is achieved with far smaller pressure since the outer skin-layer is soft gel with the yield stress $\sigma_y \sim 1$ kPa, two orders of magnitude lower than plant cell walls with $\sigma_y \sim 100$ kPa (36). Tip-growing CA precipitate exhibits higher lengthening rate than plant cells even with far smaller pressure, achieving energy efficient growth.

Control of Size and Growth Direction. Size control of the growing precipitate via flow rate modulation is even possible during the growth and is perfectly reversible with no hysteresis. As shown in Fig. 3*A*, when the flow rate is altered during extrusion, the precipitate's soft tip changes in size as the internal pressure varies (Movie S1). However, the size of the opaque cylinder, which has already undergone phase separation, is not affected. These growing characteristics allow us to build a multistepped cylinder with precisely controlled diameters. Using a dumbbell-shaped rod made by controlling the flow rate during extrusion, we conducted a tensile test to characterize the mechanical property of the tip-grown object (*SI Appendix*, Supplementary Discussion S11).

Because the internal pressure drives the tip growth, the weakest part of the tip that expands the most determines the growing direction. Therefore, tip-growing cells subtly regulates the cell wall strength at the tip to change its growing direction (37, 38). Similarly, tropism is observed in the tip-growing precipitate when an applied external stimulus shifts the weakest position, and sensing ability is structurally embedded. Without any artificial intervention, as CA–acetone solution is lighter than the surrounding water, the fresh solution at the tip tends to flow against gravity, implying that the apex of the tip is weakest. This corresponds to the negative gravitropism, and Fig. 3*B* shows that the tip keeps growing in the direction of buoyancy even after the nozzle extruding CA solution is rotated (Movie S2). Defining the growth angle θ as the angle between the growth direction and the horizontal line, θ remains as 90° even when the nozzle is rotated ($\alpha = 0°$ to 90°). When the density of the solution is higher than the surrounding water, the precipitate grows in the direction of gravity, exhibiting positive gravitropism (*SI Appendix*, Supplementary Discussion S12).

Besides gravity, we can actively steer the growing precipitate using light by adding photoinitiator, camphorquinone (CQ), coinitiator, ethyl-4-(dimethylamino)benzonate (EDMAB), and cross-linker of poly(ethylene glycol) diacrylate (PEGDA), to the solution. These additives cause polymerization of the monomer when irradiated by light with 450 nm wavelength (39). When the tip is subjected to a local photostimulus of laser sheet, generated by splitting laser beam with plano-concave cylindrical lens (LK1336RM, Thorlabs), wall strength is locally modulated as the light-shed part stiffens. With the growth ceased at the stiffened part, the tip changes direction by growing from the shaded region. As shown in Fig. 3*C*, when the precipitate originally growing against gravitational direction encounters a tilted laser sheet, it grows along the laser sheet ($\theta = 65°$), exhibiting phototropism. When the laser is turned off, the growing precipitate recovers the original negative gravitotropism ($\theta = 90°$) at $t = 260$ s (Movie S2).

The growing precipitate can passively interact with the surrounding environments through mechanical contact without being damaged thanks to soft gel covering the tip. When the growing tip contacts a hydrophilic porous mechanical obstacle (*SI Appendix*, Supplementary Discussion S13), although the growth is ceased at the contact spot, neighboring region can still grow leading the precipitate to change direction. Fig. 3*D* shows precipitate encountering mechanical obstacle, a tilted hydrophilic foam, grows along the foam ($\theta = 30°$) (Movie S2).

Thigmotropism enables the precipitate to autonomously sense and bypass obstacles. As shown in Fig. 4*A*, when the tip-growing precipitate enters a forest of pillars of hydrophilic foam, the precipitate smoothly makes its way through the obstacles, a result of combination of thigmotropism and gravitropism (Movie S3). However, when a basal-growing polymeric solution, 30 wt% CA–acetone solution, encounters an identical pillar array, it buckles and coils after initial contact rather than bypassing the obstacles as shown in Fig. 4*B*.

Thigmotropism also enables the growing precipitate to solve mazes autonomously. Fig. 4*C* shows the precipitate solving a maze comprising dead ends and an exit after corners. Although the precipitate entering the maze at $t = 0$ may first enter a dead end at $t = 8$ min, it can sense the dead end, change direction, return to the crossroad ($t = 14$ min), and eventually solve the maze ($t = 20$ min). This ability is owing to the precipitate's tendency to seek a path of minimal resistance to its growth. Similarly, when the tip of a growing precipitate encounters the edge of an obstacle, it can split into two branches. However, growth is soon ceased at the smaller branch and only the larger one keeps growing since the internal solution tends to flow toward the larger branch where it will experience less resistance.

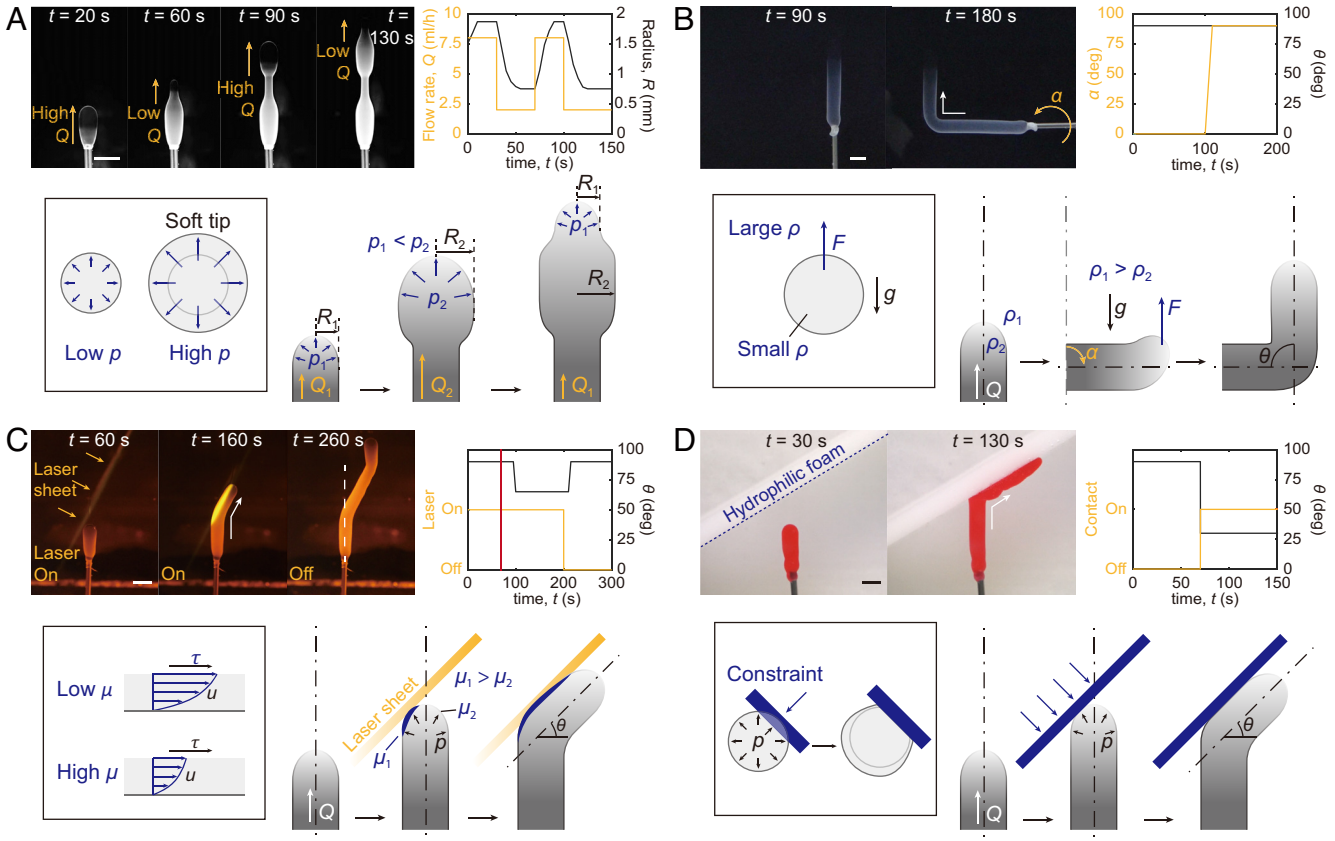

Fig. 3. Size control and tropism in the tip-growing precipitate. (*A*) In situ size modulation of a growing cylinder. The thick and thin parts are made by extruding the solution with flow rates of 8 and 2 mL/h, respectively. The black line in the graph denotes the radius of the growing tip, *R*, and the yellow line denotes flow rate. (*B*) Gravitropism of growing CA precipitate. Although a nozzle from which the solution is extruded is rotated 90° at 100 s ($\alpha = 90°$), the tip keeps growing in the direction of buoyancy ($\theta = 90°$). The black line in the graph denotes growing angle, and yellow line denotes the rotated angle of the nozzle. (*C*) Phototropism of the growing CA precipitate. By partially shedding light on the tip using a laser sheet, the growing precipitate can be remotely guided. Polymerization occurring at the light-shed part of the tip locally increases the viscosity ($\mu_1 > \mu_2$), and ceases the growth. Original growing direction is denoted by white dotted line and laser sheet is denoted by yellow arrows. The yellow line in the graph denotes on-off status of the laser, the red line denotes the time when the growing precipitate first encounters the laser sheet, and the black line denotes growing angle. (*D*) Thigmotropism of growing CA precipitate. When the precipitate contacts an inclined hydrophilic foam, it changes direction to grow along the obstacle. Red dye was added to the solution to enhance contrast. The yellow line in the graph denotes the contact status, and black line denotes growing angle. White arrows in the pictures denote reorientation of growth direction in response to the external stimuli (*B*, *C*, and *D*). (Scale bars, 5 mm (*A*–*D*).)

We finally demonstrate the possible applications of our growing polymeric precipitation system. First, exploiting its capability to sense the direction of external force, the precipitate can print a 3D structure inside a confined space. Conventional extrusion-based 3D printing techniques, such as fused deposition modeling (40) or direct ink writing (41), require adequate space for the printing nozzle to freely move. On the contrary, we can make the precipitate to grow into a specific shape from a fixed nozzle, by rotating the system. For example, Fig. 4*D* shows a spiral of CA printed inside a vial, which is built by rotating the axially tilted vial during extrusion, utilizing the negative gravitropism of the growing precipitate. We can control the diameter of the spiral by changing the angular velocity, such that for solution extruded with flow rate of 8 mL/h, large angular velocity (0.93 rpm) results in small diameter (6 mm) and small angular velocity (0.54 rpm) results in large diameter (10 mm) as illustrated in Fig. 4*D*.

Typical tip-growing plant cells act as a channel, through which materials are transported, e.g., pollen tubes transport sperm cells from the pollen to the ovule, and root hairs uptake nutrition and water from the soil. Inspired by these biological functions, we suggest our growing precipitate tube as a material transporting channel. The significantly low permeability of the precipitate wall is discussed in *SI Appendix*, Supplementary Discussion S14. Just by replacing the fresh CA–acetone solution with another fluid, the tube can serve as the fluid conduit. As shown in Fig. 4*E*, when the internal fluid is switched to liquid metal (eutectic Ga-In alloy), the CA tube guides a growing conductive wire that can complete an electric circuit from a battery to an LED (light emitting diode) bulb (Movie S3). To do so, the precipitate first grows from the nozzle toward the lead (t = 80 s). Once the precipitate touches the lead, liquid metal, instead of CA–acetone solution, is fed through the nozzle. Since the precipitate is nonconductive, the LED bulb is not lit when only the precipitate contacts the lead (t = 270 s). However, when the transported liquid metal touches the lead, the bulb is lit (t = 300 s). In this manner, materials heavier than its surrounding media can be transported against gravity while electrically insulated by the polymeric sheath.

The solidified wall of CA is capable of transporting water-miscible liquid in water (Movie S3). In Fig. 4*F*, the growing precipitate is guided using a laser sheet toward a target (t = 4 min), an open end of a glass tube situated just below the free surface of water in the bath. By modulating the flow rate, the diameter of the tube was reduced from 3.8 mm in the beginning to 2.0 mm before entering the glass tube and then increased again to 5.0 mm to enable tight fitting with the glass tube (t = 15 min). Then,

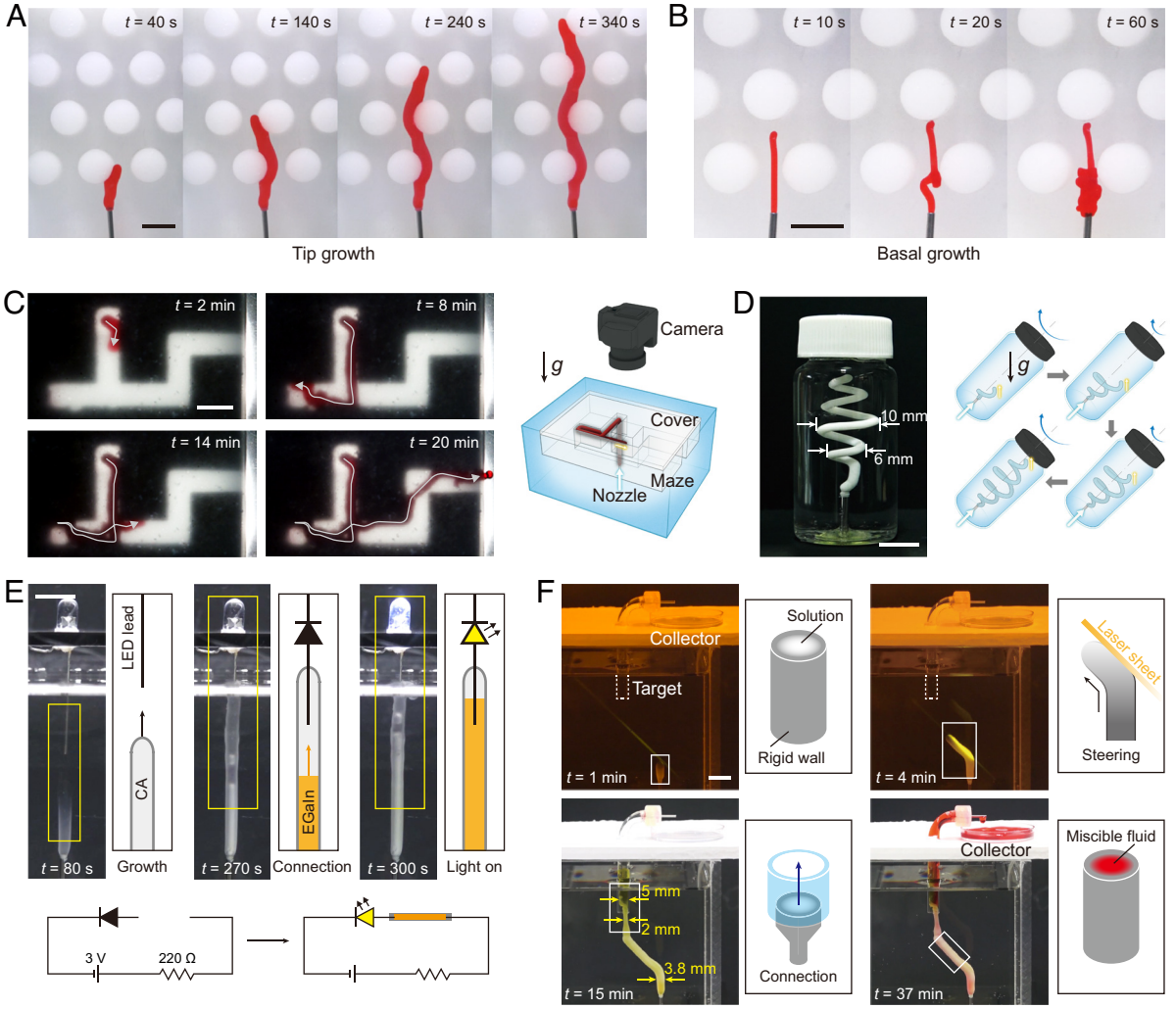

Fig. 4. Autonomous exploration and applications of the tip-growing precipitate. (*A*) Tip-growing polymeric solution bypassing a pillar array of hydrophilic foam. Negative gravitropism and negative thigmotropism of the tip-growing precipitate enables the precipitate to make its way through the pillar array without external intervention. (Scale bar, 10 mm.) (*B*) Basal-growing solution (30 wt% CA–acetone solution) encountering a pillar array. Unlike tip-growing solution, basal-growing solution is blocked by the pillars. (Scale bar, 10 mm.) (*C*) Tip-growing precipitate autonomously solving a maze through growth. Trajectory of the growing solution is denoted by gray lines. The schematic of experimental setup is shown next to the images, where the maze patterned foam is covered with a thin hydrophilic foam. (Scale bar, 10 mm.) (*D*) A spiral built inside a vial exploiting negative gravitropism. The schematic of the experiment is shown next to the image, where the size of the blue arrows denotes the magnitude of the angular velocity. (Scale bar, 5 mm.) (*E*) Growing precipitate used as a conduit of liquid metal to connect a battery (outside the picture) and a submerged lead of the LED. The LED bulb is lit only when the transported liquid metal contacts the lead at $t = 300$ s. The schematic right to each picture illustrates the connection status, and the overall circuit diagrams are shown below the pictures. (Scale bar, 5 mm.) (*F*) Shaped growth of the precipitate for transport of water-miscible liquids in water. The water-miscible acetone–ethanol mixture is collected at the container above the water bath at $t = 37$ min.

water-miscible acetone–ethanol mixture (colored with red dye) is extruded into the CA tube and finally collected at a container above the water bath ($t = 37$ min).

Conclusions

We have reported tropic tip growth of polymeric precipitate from CA–acetone solution extruded in water, which is able to sense multiple stimuli and change its growing direction accordingly. Sharing identical underlying physical mechanism in growth, the shape of growing polymeric precipitate resembled that of tip-growing cells in nature while the artificial system grew in a highly energy efficient manner compared to the cells. With the position of weakest part at the tip determining the growing direction, the precipitating system exhibited negative gravitropism and thigmotropism. By adding photosensitive additives to the solution, we imposed negative phototropism on the growing solution. These tropic characteristics enabled the growing polymer precipitate to perform various tasks including printing 3D structures in a confined space, sensing and bypassing mechanical obstacles or mazes, and transporting another liquid through water.

Stimuli-responsive systems that can grow in a tropic manner can pave a pathway to artificially realizing various biological functions observed in plants and fungi. In addition, because the system is based on a polymer solution, various materials can be mixed or dissolved to enhance the responsivity or functionality of the system. For instance, phase separation front can be remotely guided using magnetic field by adding ferromagnetic particles to the solution.

Unlike rigid robots that require both sensors and actuators to interact with their surrounding environments, our system is capable of perceiving environmental changes without sensory parts thanks to its pressure-driven growth mechanism that structurally

embeds the sensing ability. Soft mechanical systems capable of versatile adaption to the surrounding environments as demonstrated in this work will enrich soft robotic technologies armored with physical intelligence (42).

Materials and Methods

Materials. CA–acetone solution was prepared by dissolving CA (Sigma-Aldrich) in acetone. The concentration of CA in the solution varied from 10 wt% to 35 wt%, and the polymeric solution was extruded using a syringe pump (LSP04-1A, Longer Precision Pump). When visualizing the internal flow, 0.5 wt% fluorescent particles (PS-FluoRed-10.0, microparticles GmbH) were added to the solution. In some experiments, Oil Red O (Sigma-Aldrich) was added to the polymer solution for visualization purposes. In phototropism experiments, CQ (Sigma-Aldrich), EDMAB (Sigma-Aldrich), and PEGDA (Sigma-Aldrich, average Mn ~ 700) were added to the solution. The composition of the photo-responsive solution was 16 wt% CA, 56 wt% acetone, 2 wt% CQ, 2 wt% EDMAB, and 24 wt% PEGDA, and when using the photo-responsive solution, 20 wt% acetone–water solution was used as a surrounding liquid. EGaIn used in liquid transport experiment was purchased from Thermo Fisher Scientific.

Gravitropism Experiment. For the experiment shown in Fig. 3*B*, the nozzle was attached to a rotary stage. The rotary stage was then submerged in a bath of water, and CA–acetone solution was extruded through the nozzle. During the extrusion, the stage was rotated 90° counterclockwise. After the rotation, the precipitate started to grow in the direction of buoyancy at the tip.

For the experiment shown in Fig. 4*D*, first the nozzle was inserted and fixed on the bottom of the vial before water was filled in the vial. CA–acetone solution was then extruded through the nozzle. During the extrusion, the vial was rotated to guide the growing precipitate.

Phototropism Experiment. For the experiments shown in Fig. 3*C*, a tilted laser sheet was generated on the path of growing precipitate using a 450-nm laser with power of 1 W and a plano-concave cylindrical lens. When the precipitate originally growing in the direction of buoyancy entered the laser sheet, it started to grow along the sheet. The tip-growing precipitate recovered its original growing direction when the laser was turned off. The growing direction of the precipitate was guided by changing the tilted angle of the laser sheet.

Thigmotropism Experiment. For the experiments shown in Figs. 3*D* and 4 *A*, *B*, and *C*, hydrophilic melamine foam was patterned using a laser cutter. Patterns of inclined plate (Fig. 3*D*), pillar arrays (Fig. 4 *A* and *B*), and maze (Fig. 4*C*) were engraved in the foam, respectively. The patterned foam was placed on the path of the growing precipitate, and when the tip of the growing precipitate contacted the foam, it changed the growing direction.

Liquid Transport Experiment. For the experiments shown in Fig. 4*E*, the cathode lead of the LED was connected to a 220 Ω resistor and cathode of 3 V battery. The anode lead of the LED was placed on the water bath above the nozzle. The nozzle was connected to a T-shaped fitting, whose other two branches were connected to a syringe filled with polymer solution and EGaIn, respectively. The syringe containing EGaIn was connected to the anode of the battery using a jumper wire. Through the nozzle, first the CA–acetone solution was extruded to connect the nozzle and the anode lead, then EGaIn was extruded to replace the fresh CA–acetone solution inside the grown tube. Because CA is an insulator with the dielectric constant of about 5, LED was not turned on when the growing precipitate contacted the lead, but when conductive EGaIn contacted the lead, the electric circuit was completed and LED was turned on.

For the experiments shown in Fig. 4*F*, the nozzle was attached to the open end of the 90° bent glass tube with inner diameter of 5 mm. The glass tube was fixed on the plate that covers the liquid bath, and the nozzle connected to the tube was placed above the petri dish on the plate. The other end of the glass tube was placed inside the bath of acetone–water solution. Using a T-shaped fitting, the nozzle placed on the bottom of the bath, from which the polymer was extruded, was connected to two syringes filled with photo-responsive polymer solution and 20 wt% acetone–ethanol solution, respectively. Photo-responsive polymer solution was initially extruded from the nozzle, and during the growth, the precipitate was remotely guided toward the glass tube using a laser sheet. To enter the tube, the diameter of the precipitate was reduced by reducing the flow rate. After the entrance, the diameter was increased to tightly fit in the tube and extruded liquid was switched to acetone–ethanol solution. Through continuous extrusion of the acetone–ethanol solution, this water-miscible liquid was transported through the grown tube and was collected on the petri dish.

Tip-Growing Cell Data. Tip-growing cell data were obtained from the literature. The turgor pressure that drives the growth P and lengthening rate τ^{-1} of the data presented in Fig. 2*D* are provided in *SI Appendix*, Table S1.

Data, Materials, and Software Availability. All study data are included in the article and/or *SI Appendix*.

ACKNOWLEDGMENTS. We acknowledge Dongjo Kim for his help in acquiring plant images. This work was supported by National Research Foundation of Korea (Grant nos. 2018052541, 2021M3F7A1017476, 2021R1A4A3027074, and 2018M3A7B4089670). H.-Y.K. acknowledges administrative support from SNU-IAMD.

Author affiliations: [a]Department of Mechanical Engineering, Seoul National University, Seoul 08826, Korea; [b]Department of Mechanical Engineering, Ajou University, Suwon 16499, Korea; [c]Department of Materials Science and Engineering, Seoul National University, Seoul 08826, Korea; [d]Department of Mechanical Engineering, Gachon University, Seongnam 13120, Korea; and [e]Research Institute of Advanced Materials, Seoul National University, Seoul 08826, Korea

1. A. Kotikian *et al.*, Untethered soft robotic matter with passive control of shape morphing and propulsion. *Sci. Robot.* **4**, eaax7044 (2019).
2. W. Hu, G. Z. Lum, M. Mastrangeli, M. Sitti, Small-scale soft-bodied robot with multimodal locomotion. *Nature* **554**, 81–85 (2018).
3. E. Acome *et al.*, Hydraulically amplified self-healing electrostatic actuators with muscle-like performance. *Science* **359**, 61–65 (2018).
4. B. Shin *et al.*, Hygrobot: A self-locomotive ratcheted actuator powered by environmental humidity. *Sci. Robotics* **3**, eaar2629 (2018).
5. X. Qian *et al.*, Artificial phototropism for omnidirectional tracking and harvesting of light. *Nat. Nanotechnol.* **14**, 1048–1055 (2019).
6. Y. Kim, G. A. Parada, S. Liu, X. Zhao, Ferromagnetic soft continuum robots. *Sci. Robot.* **4**, eaax7329 (2019).
7. M. T. Morita, Directional gravity sensing in gravitropism. *Annu. Rev. Plant Biol.* **61**, 705–720 (2010).
8. C. W. Whippo, R. P. Hangarter, Phototropism: Bending towards enlightenment. *Plant Cell* **18**, 1110–1119 (2006).
9. K. Okada, Y. Shimura, Reversible root tip rotation in Arabidopsis seedlings induced by obstacle-touching stimulus. *Science* **250**, 274–276 (1990).
10. S. J. Gerbode, J. R. Puzey, A. G. McCormick, L. Mahadevan, How the cucumber tendril coils and overwinds. *Science* **337**, 1087–1091 (2012).
11. D. J. Cosgrove, Growth of the plant cell wall. *Nat. Rev. Mol. Cell Biol.* **6**, 850–861 (2005).
12. T. I. Baskin, Anisotropic expansion of the plant cell wall. *Annu. Rev. Cell Dev. Biol.* **21**, 203–222 (2005).
13. C. M. Rounds, M. Bezanilla, Growth mechanisms in tip-growing plant cells. *Annu. Rev. Plant Biol.* **64**, 243–265 (2013).
14. A. Geitmann, How to shape a cylinder: Pollen tube as a model system for the generation of complex cellular geometry. *Sex. Plant Reprod.* **23**, 63–71 (2010).
15. J. G. Wijmans, J. P. B. Baaij, C. A. Smolders, The mechanism of formation of microporous or skinned membranes produced by immersion precipitation. *J. Membr. Sci.* **14**, 263–274 (1982).
16. A. J. Reuvers, C. A. Smolders, Formation of membranes by means of immersion precipitation part ii. the mechanism of formation of membranes prepared from the system cellulose acetate-acetone-water. *J. Membr. Sci.* **34**, 67–86 (1987).
17. H. Strathmann, K. Kock, P. Amar, The formation mechanism of asymmetric membranes. *Desalination* **16**, 179–203 (1975).
18. A. J. Reuvers, J. W. A. van den Berg, C. A. Smolders, Formation of membranes by means of immersion precipitation part ii. The mechanism of formation of membranes prepared from the system cellulose acetate-acetone-water. *J. Membr. Sci.* **34**, 45–65 (1987).
19. S. Bartnicki-Garcia, C. E. Bracker, G. Gierz, R. López-Franco, H. Lu, Mapping the growth of fungal hyphae: Orthogonal cell wall expansion during tip growth and the role of turgor. *Biophys. J.* **79**, 2382–2390 (2000).
20. P. D. Griswold, J. A. Cuculo, An experimental study of the relationship between rheological properties and spinnability in the dry spinning of cellulose acetate-acetone solutions. *J. Appl. Polym. Sci.* **18**, 2887–2902 (1974).
21. R. Benkert, G. Obermeyer, F. W. Bentrup, The turgor pressure of growing lily pollen tubes. *Protoplasma* **198**, 1–8 (1997).
22. A. Tripathi, M. Ago, S. A. Khan, O. J. Rojas, Heterogeneous acetylation of plant fibers into micro- and nanocelluloses for the synthesis of highly stretchable, tough, and water-resistant co-continuous filaments via wet-spinning. *ACS Appl. Mater. Interfaces* **10**, 44776–44789 (2018).
23. A. Idris, M. Y. Noordin, A. F. Ismail, S. J. Shilton, Study of shear rate influence on the performance of cellulose acetate reverse osmosis hollow fiber membranes. *J. Membr. Sci.* **202**, 205–215 (2002).

24. J. Su, Q. Yang, J. F. Teo, T. S. Chung, Cellulose acetate nanofiltration hollow fiber membranes for forward osmosis processes. *J. Membr. Sci.* **355**, 36–44 (2010).
25. P. C. Hickey, D. J. Jacobson, N. D. Read, N. L. Glass, Live-cell imaging of vegetative hyphal fusion in *Neurospora crassa*. *Fungal Genet. Biol.* **37**, 109–119 (2002).
26. I. E. de la Providencia, F. A. de Souza, F. Fernández, N. S. Delmas, S. Declerck, Arbuscular mycorrhizal fungi reveal distinct patterns of anastomosis formation and hyphal healing mechanisms between different phylogenic groups. *New Phytol.* **165**, 261–271 (2005).
27. J. Dumais, S. L. Shaw, C. R. Steele, S. R. Long, P. M. Ray, An anisotropic-viscoplastic model of plant cell morphogenesis by tip growth. *Int. J. Dev. Biol.* **50**, 209–222 (2006).
28. O. Campàs, L. Mahadevan, Shape and dynamics of tip-growing cells. *Curr. Biol.* **19**, 2102–2107 (2009).
29. J. A. Lockhart, An analysis of irreversible plant cell elongation. *J. Theor. Biol.* **8**, 264–275 (1965).
30. A. J. McHugh, D. C. Miller, The dynamics of diffusion and gel growth during nonsolvent-induced phase inversion of polyethersulfone. *J. Membr. Sci.* **105**, 121–136 (1995).
31. M. B. Roller, Rheology of curing thermosets: A review. *Polym. Eng. Sci.* **26**, 432–440 (1986).
32. A. Lee *et al.*, Fabrication of slender elastic shells by the coating of curved surfaces. *Nat. Commun.* **7**, 11155 (2016).
33. E. W. Hawkes, L. H. Blumenschein, J. D. Greer, A. M. Okamura, A soft robot that navigates its environment through growth. *Sci. Robot.* **2**, eaan3028 (2017).
34. L. J. Winship, G. Obermeyer, A. Geitmann, P. K. Hepler, Under pressure, cell walls set the pace. *Trends Plant Sci.* **15**, 363–369 (2010).
35. J. K. E. Ortega *et al.*, A comparison of cell-wall-yielding properties for two developmental stages of *Phycomyces sporangiophores*. *Planta* **183**, 613–619 (1991).
36. P. B. Green, R. O. Erikcson, J. Buggy, Metabolic and physical control of cell elongation rate. *Plant Physiol.* **47**, 423–430 (1971).
37. J. Bove *et al.*, Magnitude and direction of vesicle dynamics in growing pollen tubes using spatiotemporal image correlation spectroscopy and fluorescence recovery after photobleaching. *Plant Physiol.* **147**, 1646–1658 (2008).
38. D. D. Thomson *et al.*, Contact-induced apical asymmetry drives the thigmotropic responses of *Candida albicans* hyphae. *Cell. Microbiol.* **17**, 342–354 (2015).
39. E. K. U. Larsen, N. B. Larsen, K. Almdal, Multimaterial hydrogel with widely tunable elasticity by selective photopolymerization of peg diacrylate and epoxy monomers. *J. Polym. Sci. Part B: Polym. Phys.* **54**, 1195–1201 (2016).
40. O. A. Mohamed, S. H. Masood, J. L. Bhowmik, Optimization of fused deposition modeling process parameters: A review of current research and future prospects. *Adv. Manuf.* **3**, 42–53 (2015).
41. J. A. Lewis, Direct ink writing of 3d functional materials. *Adv. Funct. Mater.* **16**, 2193–2204 (2006).
42. M. Sitti, Physical intelligence as a new paradigm. *Extreme Mech. Lett.* **46**, 101340 (2021).

Supplementary Information for
Plant cell-like tip-growing polymer precipitate with structurally embedded multi-stimuli sensing ability

Chan Jin Park, Jonghyun Ha, Hae-Ryung Lee, Keunhwan Park, Jeong-Yun Sun, and Ho-Young Kim

This PDF file includes:

Other supplementary materials for this manuscript include the following:

S1. Precipitation from the CA-acetone solution

When fresh CA-acetone solution is extruded in a bath of water, the solvent (acetone) immediately diffuses out at the solution-water interface. The rapid depletion of solvent leads to instantaneous gelation of the solution at the interface, which results in a thin, dense non-porous skin layer. Through the skin layer, the outward diffusion of solvent (acetone) and the inward diffusion of non-solvent (water) occur simultaneously, as illustrated in Fig. 2(a). The diffusion driven solvent–non-solvent exchange alters the concentration of the internal fresh solution, in a way that solute concentration increases, solvent concentration decreases, and non-solvent concentration increases with increasing water contact time. When the concentration of the solution crosses the binodal, the solution is separated into a polymer rich phase and a polymer lean phase (liquid-liquid phase separation) [S1]. After drying, the former becomes solid matrix while the latter forms a void, resulting in a porous solid as shown in the SEM image of Fig. 2(a). When liquid-liquid phase separation occurs, the initially transparent solution turns opaque as observed in the stalk of the growing precipitate.

S2. Verification of the orthogonal growth at the tip

To verify whether the precipitate grows perpendicular to the interface at the tip, we compared the experimentally obtained particle trajectories to those modeled by orthogonal growth assumption. We first calculate theoretical trajectory of the particles under the orthogonal growth assumption Initially (t_0), an arbitrary point near the apex of the tip, P_0, is chosen and the normal vector is calculated at this point. The normal vector can be calculated since the tip shape is always similar to a prolate spheroid with the major axis 1.3 time longer than the minor axis in this particular process condition. Then, the intersection point of this normal vector and the tip at the next time step t_1, P_1, becomes the position of the material point at t_1, and the line connecting the two points is the trajectory of the material point from time t_0 to t_1 under the orthogonal growth assumption. Repeating this step, we can obtain the theoretical trajectory which ends once the material point reaches the periphery of the tip. The theoretical trajectory is determined by the geometry of the tip, and the growth velocity only determines the time required to travel the trajectory.

We then quantitatively verify whether the experimentally obtained particle trajectories match the theoretically obtained ones. We calculated the coefficient of determination (R^2) between the experimental trajectories and our theoretical model shown in Fig. S1(b). For each line shown in Fig. S1(b), R^2 exceeds 0.98, implying that our theoretical model well predicts the experimental results.

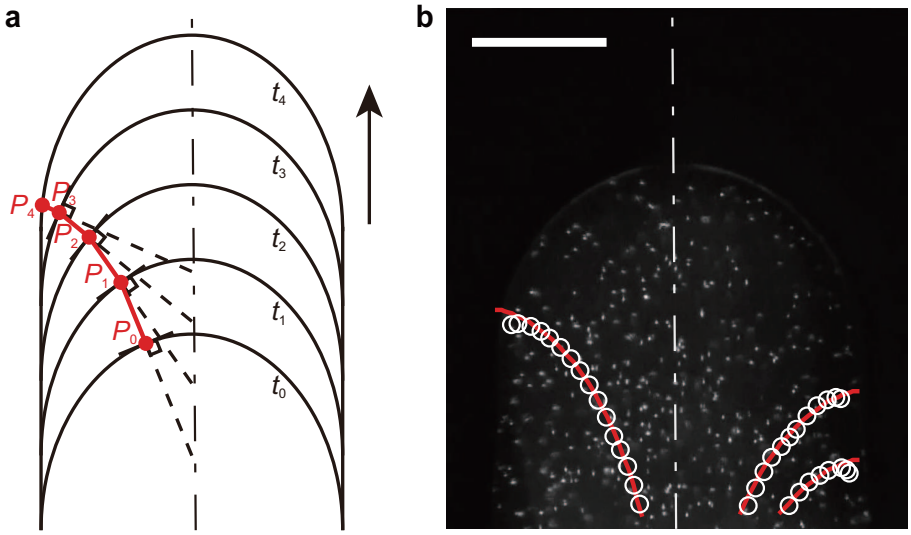

FIG. S1: **Particle trajectories near the growing tip surface.** **a**, Calculation of theoretical particle trajectory. Red circles denote the position of material point P_i at each time step t_i, and red line denotes the trajectory of the particle. **b**, Experimentally obtained particle trajectories. White circles denote the experimental position of particle at each time step, and red lines denote theoretical trajectories based on the orthogonal growth assumption. CA-acetone solution with CA concentration of 20 wt% was extruded at the flow rate of 1 ml/h. Scale bar, 500 μm.

S3. Growth behavior of polymeric solutions other than CA-acetone

To investigate growth behavior of polymeric solutions other than CA-acetone, we first varied the solvent of the solution. While using CA with average Mn~30,000 as a solute, instead of acetone, two mixtures of acetone and N,N-dimethylacetamide (DMAc), weight ratio of 2:1 and 1:2, were used as a solvent. The solute concentration was fixed as 20 wt%, and both solutions were extruded in a bath of water. When the weight ratio of acetone and DMAc was 2:1, the extruded solution exhibited tip growth. However, when the weight ratio of acetone and DMAc was 1:2, the extruded solution exhibited basal growth, implying too fast solidification near the nozzle. This is because polymeric solution with high DMAc content in the solvent requires only a small amount of non-solvent for phase separation to occur [S2]. In other words, phase separation immediately occurs in solution with high DMAc content in the solvent, which results in basal growth.

Second, we varied the polymer used as the solute. We used polysulfone (PSf) and polyvinylidene fluoride (PVDF), as a solute. For the solvent, we again used two mixtures of acetone and DMAc (weight ratio of 2:1 and 1:2). The solute concentration was fixed as 20 wt%, and both solutions were extruded in a bath of water. PSf did not dissolve in the solvent when the weight ratio of acetone and DMAc was 2:1. 20 wt% PSf-acetone-DMAc solution with acetone and DMAc weight ratio of 1:2 resulted in basal growth. On the other hand, PVDF dissolved in both mixtures of acetone and DMAc. Similar to PSf, basal growth was observed in PVDF-acetone-DMAc solution when the weight ratio of the acetone and DMAc was 1:2. However, when weight ratio of the acetone and DMAc was 2:1, the PVDF-acetone-DMAc solution exhibited tip growth.

From the experimental results, we can conclude that tip growth of precipitate can be achieved by extruding polymeric solutions that (i) undergo NIPS and (ii) require large amount of non-solvent to achieve phase separation in a bath of non-solvent.

S4. Bursting of tip

When the flow rate is increased during growth, the size of growing tip increases owing to the increased internal pressure. However, when the modified flow rate, or pressure, is too high for the phase separation front to withstand, the tip bursts. The failure occurs at the junction between the bulged tip and the stalk as shown in Fig. S2. It has been reported that tips of pollen tubes [S3] and root hairs [S9] also burst when the internal pressure is increased. Both the artificial and natural growing tubes burst at the junction of tip and stalk, where the sudden jump of tensile stress arises.

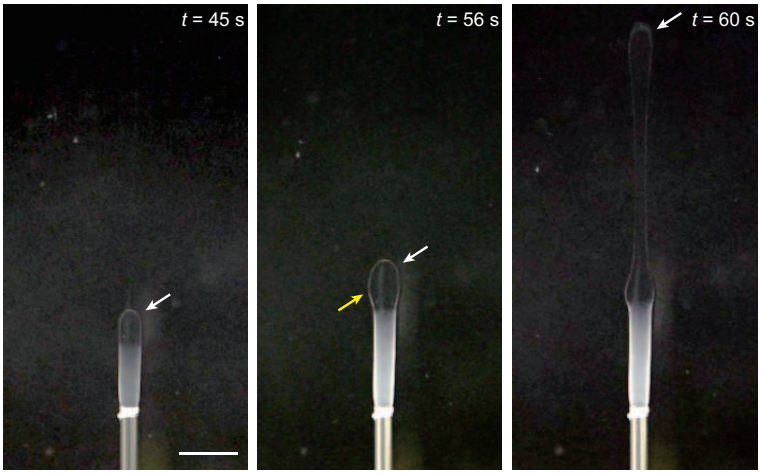

FIG. S2: **Tip bursting owing to high internal pressure.** Increasing the flow rate beyond which the precipitate can endure results in bursting of the tip. CA-acetone solution with CA concentration of 20 wt% was first extruded at the flow rate of 2 ml/h, then the flow rate was increased to 25 ml/h. Then, the tip bulges owing to the increased internal pressure (t = 56 s) and failure occurs at the junction denoted by yellow arrow between the tip and the body. The tip is separated from the stalk when failure occurs (t = 60 s). The tips are indicated by white arrows. Scale bar, 5 mm.

S5. Nozzle-independent growth

We compared the size of cylinder formed by phase separation of CA solution while varying the nozzle size. If the flow rate, which determines the internal pressure, is identical, the size of the growing cylinder is invariant regardless of the nozzle diameter. Fig. S3 shows that the nozzle size has no effect on the size or the velocity of growing precipitate.

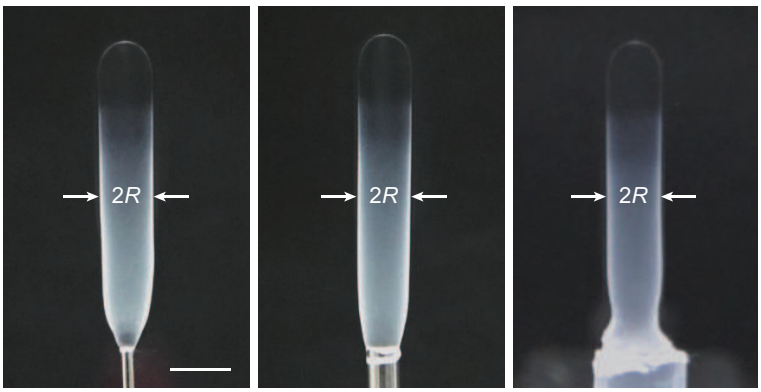

FIG. S3: **Growing precipitates extruded from different sizes of nozzles with identical flow rate.** Using the nozzles with inner diameter of 0.25, 1.07, and 2.70 mm (from left to right), CA-acetone solution with CA concentration of 25 wt% was extruded at the identical flow rate of 3 ml/h. Regardless of the nozzle diameter, growing precipitates yield identical stalk radius (R = 1.2 mm) and growing velocity (0.18 mm/s). Scale bar, 3 mm.

S6. Merging of two growing precipitates

When two growing precipitates extruded from different nozzles approach each other, their tips merge and grow as one. When the distance between the two tips are close enough, they can sense each other due to the high acetone concentration near the tip. High acetone concentration near the other tip delays the diffusion of acetone out of the solution, which makes the local strength of the wall relatively weaker. This leads the precipitates to grow towards each other, and eventually they meet and merge as shown in Fig. S4. After merging, they grow a single tip while its size is determined by the sum of the two flow rates.

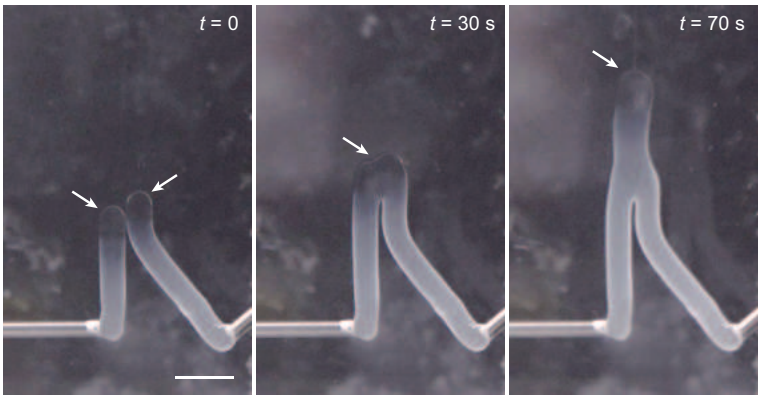

FIG. S4: **Merging of two growing precipitates.** The solution streams merge when they contact at their tips. After merging, the solutions grow a single tip (t = 70 s). The tips are indicated by white arrows. Scale bar, 3 mm.

S7. Internal pressure of growing tip

We measured the pumping pressure of CA solution by attaching the force sensor to the pusher block of the syringe pump. As the pumping speed is very low, we assumed the viscous dissipation to be negligible and internal pressure to be identical to the pumping pressure. The polymeric solution requires small gauge pressure, less than 4 kPa, to grow a tip, allowing us to neglect the yield stress necessary to initiate flow. Measured internal pressure increased with increasing flow rate, which led to increased radius of growing precipitate with an empirical relationship of $R \sim \sqrt{P}$ as shown in Fig. S5.

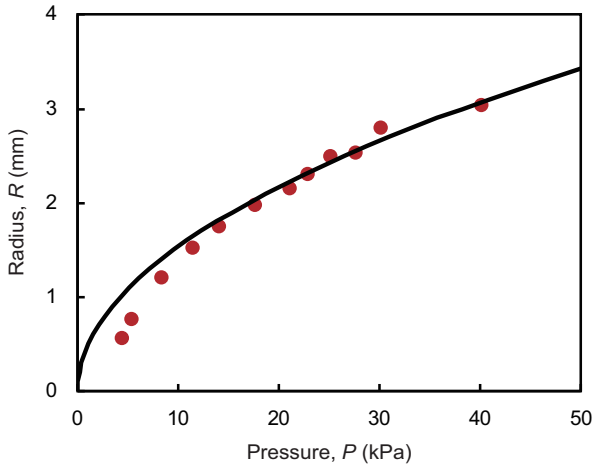

FIG. S5: **Radius of growing precipitate, R versus internal gauge pressure, P.** Red dots correspond to experimental measurement results, and black line corresponds to an empirical line, $R = 0.15\sqrt{P}$ with R in mm and P in kPa.

S8. Tip shape

We compared the tip shape of the precipitate while varying the flow rate. As shown in Fig. S6, the shapes of tip are always prolate semi-spheroid with semi-major axis (a) being 1.3 times longer than the semi-minor axis (b) regardless of the flow rate. This is because the shape of tip is solely determined by a single flow coupling variable, one of material properties, when the tip grows in an orthogonal manner [S5]. As we always used solutions composed of cellulose acetate and acetone, the tip shape is always similar.

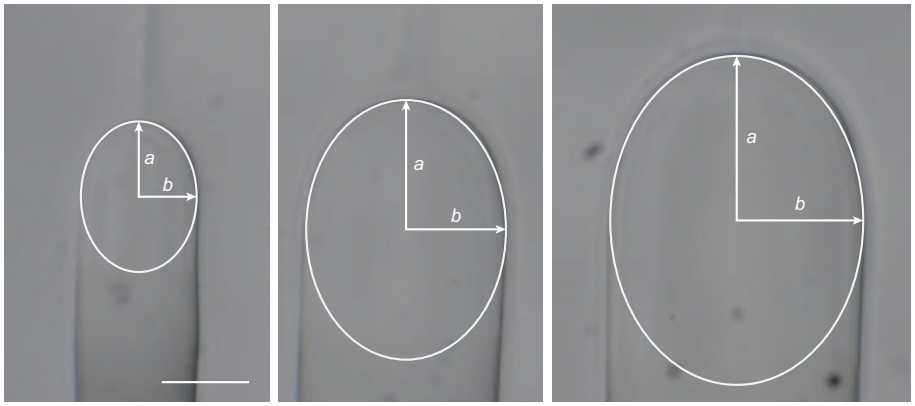

FIG. S6: **Tip shape of growing precipitates with varying flow rates.** Tips growing from different flow rates of CA solutions are overlapped with white ellipse, whose semi-major axis is 1.3 times longer than the semi-minor axis as a guide. CA-acetone solution with CA concentration of 25 wt% was extruded at the flow rates of 1, 3, and 5 ml/h (left to right). Scale bar, 1 mm.

S9. Wall thickness

We measured the wall thickness of growing precipitates. During growth, the extruded fluid was switched to liquid metal (EGaIn) to replace the fresh inner solution. Liquid metal was continuously fed until filling the entire hollow stalk. When the extrusion was finished, the precipitate was kept in water for 1 h to ensure that solvent–non-solvent exchange had fully taken place. Then it was taken out of water and liquid metal inside the solution was rinsed out to obtain a hollow cylinder of CA. Finally, the hollow cylinder was cut-open and wall thickness at varying positions was measured using an optical microscope. Fig. S7 plots wall thickness versus distance from the tip, which shows that wall thickness increases proportional to the square root of distance from the tip, or square root of water contact time because the solution grows with a constant velocity. This implies that the gel made of CA, acetone, and water, whose thickness increases with the square root of non-solvent (water) diffusion time [S6], forms the channel wall.

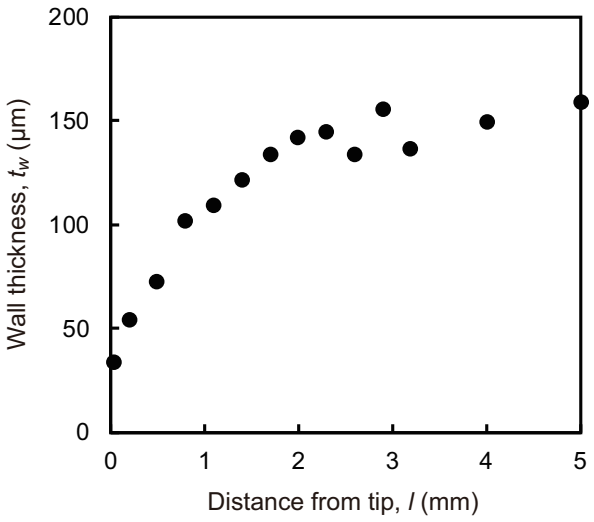

FIG. S7: **Wall thickness, t_w versus distance from the tip, l.** CA tube was fabricated by first extruding the CA-acetone solution of CA concentration 25 wt% at the flow rate of 5 ml/h, then replacing the inner solution with liquid metal.

S10. Length of the transparent region

The length of the transparent region, L, in the growing precipitate, which consists of a semi-spheroidal tip and the upper part of the cylinder near the tip, increases with increasing R as shown in Fig. S8. The experimental data for different CA concentration are collapsed to a single line of $L = 1.3R + L_c$, where $1.3R$ is the length of the transparent tip and L_c is the length of the transparent cylinder. When contacting the non-solvent (water), the initially transparent polymer solution undergoes phase separation and turns opaque when non-solvent-contact time exceeds the precipitation time t_p, which, for an immersed polymer film, increases proportional to the square of initial film thickness [S6]. For the transparent cylinder, the gel layer thickness at the equator of the tip $\delta(S)$ acts as the initial thickness because there is no influx of fresh solution to the gel layer once it is deposited at the equator. Therefore, with the precipitate growing at a constant growth rate U, L_c is calculated as $L_c = Ut_p \sim U\delta^2(S)$. This leads to $L \sim 1.3R + U\delta^2(S)$, and substituting $\delta(S) \sim \tau^{0.5}$ (Supplementary Discussion S8), we get $L \sim 1.3R + U\tau$, which matches our experimental observation.

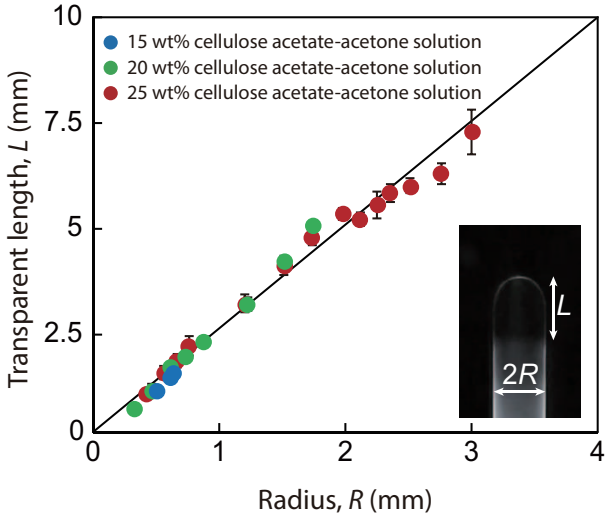

FIG. S8: **Length of the transparent region.** Experimentally measured transparent length at the tip, L versus R. Black line stands for $y = 2.5x$. Each data point is the average of three measurements, and error bars correspond to the standard deviation.

S11. Mechanical properties of the tip-grown objects

To characterize the mechanical properties of the fabricated objects, we conducted tensile test of a dumbbell-shaped specimen (Fig. S9a) using a Universal Testing System (Instron 34SC-1). The specimen was fabricated by controlling the extrusion flow rate during growth, and was placed in water for 2 days after the extrusion to ensure complete solidification. The shoulders of the specimen were attached to the slide glass, which was gripped by the apparatus, and the specimen was pulled with a constant rate of 1 mm/min until break. Inset of Fig. S9(a) shows the cross-section of the fractured specimen, revealing its porous structure. We plot a stress-strain curve of the specimen in Fig. S9(b). By measuring the initial slope of the curve, we find Young's modulus (E) to be 320.7 $\pm$ 28.4 MPa (number of samples, n = 3). We can enhance the mechanical property, E, by converting the CA to cellulose via deacetylation process [S7]. Conversion was done by immersing the CA specimen in ethanolic NaOH solution for 24 h, and the stress-strain curve of the NaOH treated specimen is shown in Fig. S9(b). The measured E (initial slope) of the NaOH treated specimen is 399.3 $\pm$ 11.1 MPa (n = 3), which is approximately 20% higher than E of the untreated specimen.

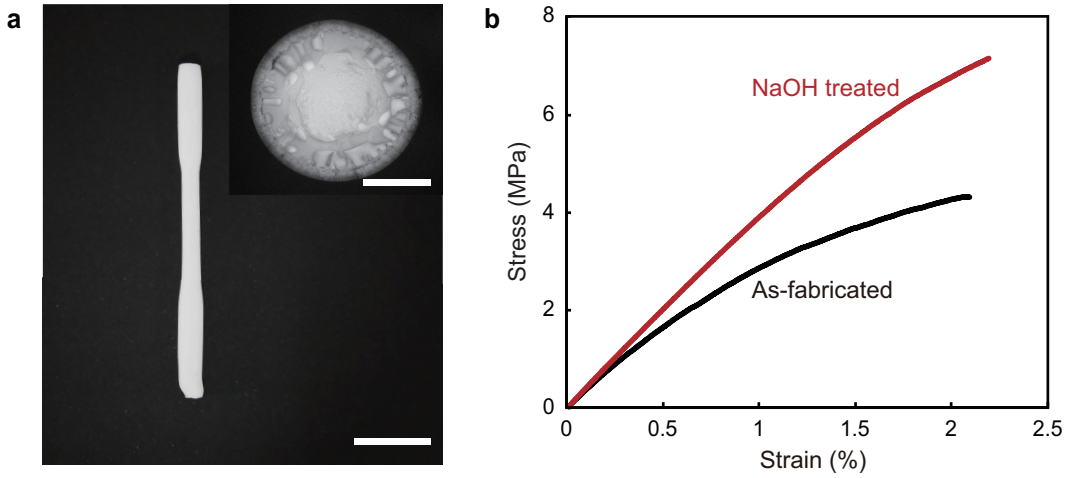

FIG. S9: **Characterization of mechanical properties. a**, A specimen used in tensile test, and a picture of a fracture surface (inset). The specimen is fabricated by first extruding the solution with extrusion flow rate of 13 ml/h, then reducing the flow rate to 6 ml/h, and then increasing the flow rate to 13 ml/h. The diameter of the specimen at the shoulder is 3.5 mm, and diameter of the gauge section is 2.5 mm. Large voids in the center and small pores near the wall are clearly visible on the fracture surface in the inset. Scale bars, 1 cm (picture), and 1 mm (inset). **b**, Stress-strain curves of dumbbell-shaped specimens. Black line denotes the result from the bare specimen, and red line denotes the result from the NaOH treated specimen.

S12. Positive gravitropism of a dense polymeric solution based precipitate

We can control the solution's density by changing the solvent. By using the mixture of acetone (ρ_a = 784 kg/m^3) and ethyl lactate (ρ_e = 1030 kg/m^3) as a solvent, we can make dense solution that is heavier than the surrounding water (ρ_w = 997 kg/m^3). In contrast to the CA-acetone solution based precipitate that exhibits negative gravitropism, the precipitate based on the precipitation of the dense solution grows in the direction of gravity, exhibiting positive gravitropism, as shown in Fig. S10.

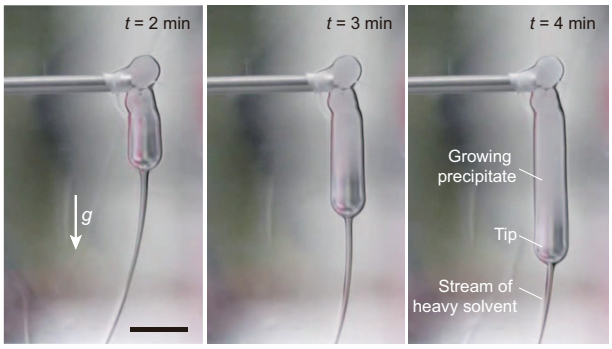

FIG. S10: **Positive gravitropism of a dense polymeric solution based precipitate.** The tip-growing precipitate grows in the direction of gravity when the polymeric solution is heavier than the surrounding liquid. A stream of heavy solvent that has diffused out of the solution flows downwards from the tip. The composition of the solution is 25 wt% CA, 18.75 wt% acetone, 56.25 wt% ethyl lactate. Scale bar, 5 mm.

S13. Effects of the surface characteristics of substrate on the post-contact behavior of the precipitate

During the tip growth, the solvent (acetone) diffuses out of the solution in the direction of buoyancy because it is lighter than water. Therefore, as shown in Fig. S11(a), when the tip-growing precipitate meets a substrate, either hydrophobic or non-porous, the solvent accumulates at the surface to form a high-solvent-concentration layer. The solvent–non-solvent exchange, which results in the wall strength gradient and directional growth of the precipitate, is inhibited in the high-solvent-concentration layer. Thus, when the tip-growing precipitate contacts hydrophobic or non-porous substrates, it does not grow in a directional manner but rather expands radially as shown in Figs. S11(b) and (c).

On the other hand, we can suppress the build-up of high-solvent-concentration layer near the surface by using hydrophilic porous substrates. As shown in Fig. S11(d), when the substrate is hydrophilic and porous, the solvent infiltrates through the pores instead of being accumulated on the substrate. Therefore, as shown in Fig. S11(e), when contacting a hydrophilic porous substrate like filter paper (or a hydrophilic foam as used in our thigmotropism experiment), the precipitate continues to grow from its tip in a directional manner, along the substrate.

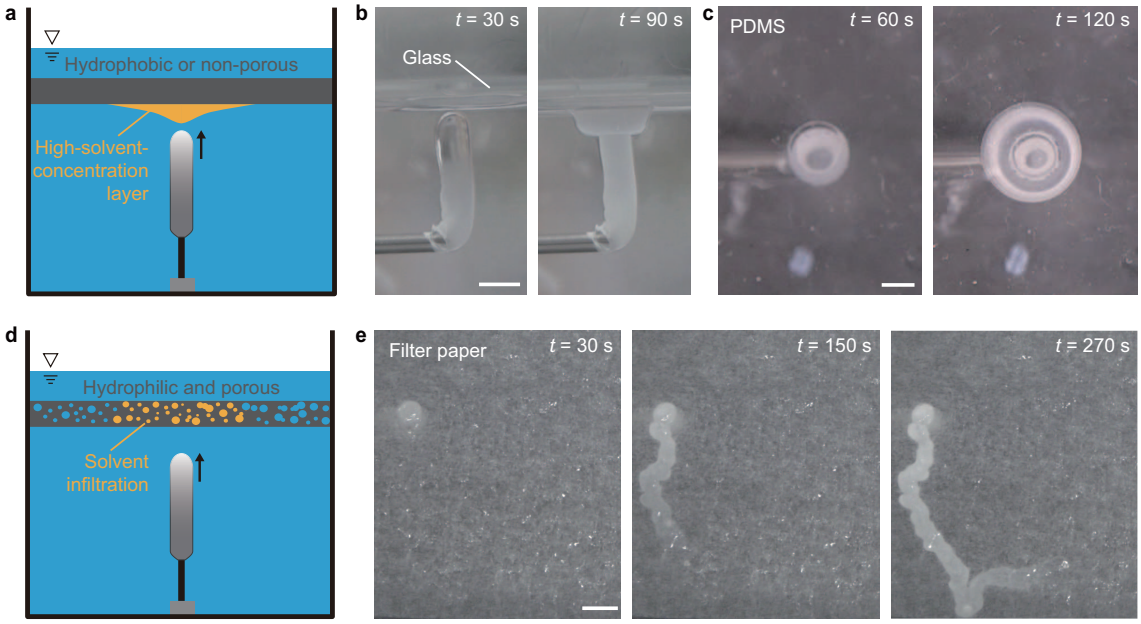

FIG. S11: **Effects of surface characteristics on the post-contact behavior of tip-growing precipitate.** **a**, Schematic of a tip-growing precipitate approaching either hydrophobic or non-porous substrate. **b**, Post-contact behavior of the tip-growing precipitate upon contacting a hydrophilic glass (side view). After the contact, the tip expands radially. **c**, Post-contact behavior of the tip-growing precipitate upon contacting a hydrophobic PDMS film (top view). Similar to b, the tip expands radially. **d**, Schematic of a tip-growing precipitate approaching a hydrophilic porous substrate. **e**, Post-contact behavior of the tip-growing precipitate against hydrophilic porous filter paper (top view). After the contact, the precipitate continues to grow from its tip along the substrate. Scale bars, 5 mm (b, c, e).

S14. Permeability of the fabricated CA tube

We measured the water permeability of the fabricated CA tube. First, by replacing the internal fresh polymeric solution with liquid metal (EGaIn) during growth (Fig. S12a), we closed the distal end of a CA tube as shown in Fig. S12(b). Then, as shown in Fig. S12(c), we attached the open end of the CA tube to a PTFE tubing, which was connected to a pressure chamber partially filled with water. The permeability of the CA tube was obtained by measuring the volume of water pressed out of the tube under the applied pressure in the chamber. Since the wall was much thinner than the closed end, water would mostly permeate the wall of the tube if any. However, no water was detected at the outside wall of the tube even when the applied gauge pressure exceeded 1 bar. This implies that the permeability of the precipitate wall is low enough to make the precipitate tube suitable for liquid transportation.

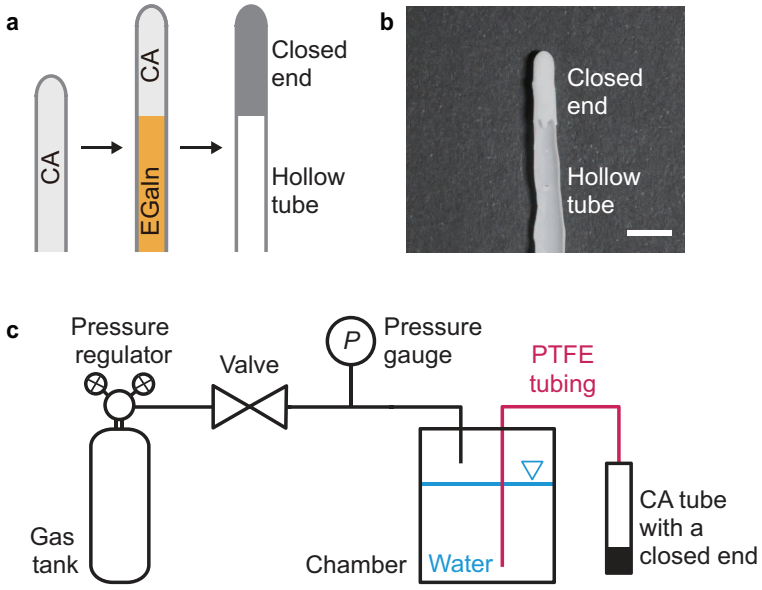

FIG. S12: **Measuring the permeability of the precipitate.** **a**, Schematic of fabricating a CA tube with a closed end. Liquid metal (EGaIn) that partially fills the CA precipitate is rinsed away after solidification. **b**, Longitudinal section of the fabricated CA tube with a closed end. CA-acetone solution with CA concentration of 25 wt% was extruded at the flow rate of 5 ml/h. After the solidification, the resulting tube was cut in half in the longitudinal direction. Scale bar, 5 mm. **c**, Schematic of experimental setup for measuring the permeability of the precipitate.

Table S1. Turgor pressure and lengthening rate of tip growing cells

Classification	Species	P (kPa)	τ^{-1} (s^{-1})	Reference
Pollen tube	*L. longiflorum*	250	0.00423	(21)
Pollen tube	*L. longiflorum*	170	0.00415	(21)
Pollen tube	*L. longiflorum*	140	0.00597	(21)
Pollen tube	*L. longiflorum*	141	0.0079	(21)
Pollen tube	*L. longiflorum*	160	0.00792	(21)
Pollen tube	*L. longiflorum*	190	0.00972	(21)
Pollen tube	*L. longiflorum*	240	0.00987	(21)
Pollen tube	*L. longiflorum*	240	0.00843	(21)
Pollen tube	*L. longiflorum*	250	0.0078	(21)
Pollen tube	*L. longiflorum*	270	0.00598	(21)
Pollen tube	*L. longiflorum*	290	0.00838	(21)
Pollen tube	*L. longiflorum*	260	0.01258	(21)
Pollen tube	*L. longiflorum*	170	0.01398	(21)
Pollen tube	*L. longiflorum*	140	0.01837	(21)
Fungus	*A. nidulans*	600	0.00333	(S8)
Fungus	*P. blakesleeanus*	480	0.00236	(35)
Fungus	*N. crassa*	111	0.01038	(S9)
Fungus	*N. crassa*	130	0.01808	(S9)
Fungus	*N. crassa*	144	0.02673	(S9)
Fungus	*N. crassa*	194	0.0336	(S9)
Fungus	*N. crassa*	249	0.03192	(S9)
Fungus	*N. crassa*	300	0.04023	(S9)
Fungus	*N. crassa*	322	0.04079	(S9)
Fungus	*N. crassa*	385	0.04344	(S9)
Fungus	*N. crassa*	400	0.04827	(S9)
Fungus	*N. crassa*	472	0.05094	(S9)
Fungus	*N. crassa*	494	0.04958	(S9)

Fungus	*N. crassa*	564	0.05465	(S9)
Water mold	*A. bisexualis*	690	0.00275	(S10)
Water mold	*S. ferax*	390	0.0439	(S11)

Captions for Movies

Movie S1 (separate file). Characteristics of tip-growing polymer precipitate

When CA-acetone solution is extruded in the bath of water, the precipitate grows from its tip, which can be noted by the tip that always remains transparent. Internal flow visualization verifies that the tip growth is internal pressure-driven, and that the fresh polymer solution is replenished at the tip. The size of the growing precipitate can be precisely modulated by controlling the flow rate.

Movie S2 (separate file). Tropic characteristics of tip-growing precipitate

When the nozzle in which the polymer solution is extruded is rotated during the extrusion, the precipitate reorients the growing direction and continues to grow in the direction of the buoyancy (negative gravitropism). When light is partially shed at the tip of the photo-responsive solution using laser sheet, the precipitate grows along the laser sheet (negative phototropism). When the growing precipitate contacts inclined plate of melamine foam, the solution changes direction and grows along the obstacle (negative thigmotropism).

Movie S3 (separate file). Applications of tip-growing precipitate

Negative gravitropism and thigmotropism enables the growing precipitate to bypass array of pillars of melamine foam without any external intervention. The grown precipitate can be used as a fluid conduit, while the solidified wall enables shielded transport. The grown precipitate can be used to transport conductive liquid metal in water and complete an electric circuit. Water-miscible liquid can also be transported in water through a non-straight path using remotely steered CA tube. Water-miscible acetone-ethanol solution is transported through water and collected in the petri dish above the water bath.

References

[S1] J. G. Wijmans, J. P. B. Baaij, C. A. Smolders, The mechanism of formation of microporous or skinned membranes produced by immersion precipitation. *J. Membr. Sci.* **14**, 263-274 (1982).

[S2] F. W. Altena, C. A. Smolders, Calculation of liquid-liquid phase separation in a ternary system of a polymer in a mixture of a solvent and a nonsolvent. *Macromolecules* **15**, 1491-1497 (1982).

[S3] R. Benkert, G. Obermeyer, F.-W. Bentrup, The turgor pressure of growing lily pollen tubes. *Protoplasma* **198**, 1-8 (1997).

[S4] R. R. Lew, Pressure regulation of the electrical properties of growing *Arabidopsis thaliana* L. root hairs. *Plant Physiol.* **112**, 1089-1100 (1996).

[S5] J. Dumais, C. Steele, S. R. Long, An anisotropic-viscoplastic model of plant cell morphogenesis by tip growth. *Int. J. Dev. Biol.* **50**, 209-222 (2006).

[S6] A. J. McHugh, D. C. Miller, The dynamics of diffusion and gel growth during nonsolvent-induced phase inversion of polyethersulfone. *J. Membr. Sci.* **105**, 121-136 (1995).

[S7] S. W. Pattinson, A. J. Hart, Additive manufacturing of cellulosic materials with robust mechanics and antimicrobial functionality. *Adv. Mater. Technol.* **2**, 1600084 (2017).

[S8] B. González-Bermúdez, Q. Li, G. V. Guinea, M. A. Peñalva, G. R. Plaza, Probing the effect of tip pressure on fungal growth: Application to *Aspergillus nidulans*. *Phys. Rev. E* **96**, 022402 (2017).

[S9] R. R. Lew, S. Nasserifar, Transient responses during hyperosmotic shock in the filamentous fungus *Neurospora crassa*. *Microbiology* **155**, 903-911 (2009).

[S10] N. P. Money, F. M. Harold, Extension growth of the water mold *Achlya*: Interplay of turgor and wall strength. *Proc. Natl. Acad. Sci. USA* **89**, 4245-4249 (1992).

[S11] F. M. Harold, R. L. Harold, N. P. Money, What forces drive cell wall expansion? *Can. J. Bot.* **73**, S379-S383 (1995).